Geoscience Letters

RESEARCH LETTER

Open Access

Seismically-induced landslide probabilistic hazard mapping of Aba Prefecture and Chengdu Plain region, Sichuan Province, China for future seismic scenarios

Xiaoyi Shao[1,2,3], Siyuan Ma[4], Chong Xu[1,2,3*], Jia Cheng[1,2] and Xiwei Xu[5]

Abstract

The purpose of this work is to carry out seismically induced landslide probabilistic hazard mapping for future seismic scenarios of Aba Prefecture and Chengdu Plain region, Sichuan Province, China. Nine earthquake events that occurred in the regions and neighboring areas are selected, which include a total of 251,260 landslide records. This work used 12 influencing factors including elevation, slope, aspect, relief, topographic wetness index (TWI), topographic position index (TPI), peak ground motion, distance to active faults, vegetation coverage, distance to roads, lithology, and annual rainfall to establish the LR model. Based on the probabilistic seismic hazard analysis (PSHA) method, the distribution of predicted seismic motion under four earthquake scenarios is calculated including frequent, occasional, rare, and very rare earthquake occurrence. Using the PGA distribution of the four scenarios as input peak ground motion parameters, we calculated the occurrence probability of coseismic landslides in the entire Aba Prefecture and Chengdu Plain region under the action of different ground motions. The result shows that the high-hazard areas are mainly concentrated in the Longmenshan fault zone, and the southern area of Kangding is also a potential high-hazard area for landsliding. Meanwhile, as the probability of exceedance decreases, the probability of corresponding earthquake-induced landslides hazard probability and the area of high-hazard regions also significantly increase. Especially, the Pengguan complex rock mass in the southwest of the Longmenshan fault zone is the potential high-hazard area for coseismic landslides.

Highlights

- Establishing a coseismic landslides evaluation model suitable for Aba Prefecture and Chengdu Plain region.
- Calculating the occurrence probability of coseismic landslides under different peak ground motions.

Keywords Earthquake-induced landslides, Aba Prefecture and Chengdu plain region, Landslide hazard assessment, Probabilistic seismic hazard analysis (PSHA), Logistic regression (LR) model

*Correspondence:
Chong Xu
xc11111111@126.com
Full list of author information is available at the end of the article

Introduction

Earthquake-induced landslides are a common type of secondary earthquake hazard in mountainous areas, and the losses they cause often account for a considerable proportion of earthquake disasters (Huang and Fan 2013; Keefer 1984). The 2008 Wenchuan earthquake triggered massive landslides that directly caused the death of 20,000 to 30,000 people, accounting for roughly 30% of total earthquake fatalities, with the Wangjiayan landslide burying half of the old Beichuan County town and causing about 1600 deaths (Cui et al. 2009; Yin et al. 2009). On May 31st, 1970, a snow avalanche caused by the Peru earthquake directly buried the city of Yungay, causing approximately 23,000 deaths. As a result, earthquake-induced landslides have received widespread attention in recent decades, and related studies have primarily focused on the construction of landslide inventories (Shao et al. 2023a, b; Zhao et al. 2021), distribution pattern (Jibson and Tanyaş 2020; Papathanassiou et al. 2021), susceptibility and hazard assessment (Lombardo et al. 2019; Robinson et al. 2017; Shao et al. 2021), and landscape evolution (Dai et al. 2021; Parker et al. 2011). Among them, earthquake-induced landslide hazard mapping plays an important role in emergency rescue and disaster recovery and reconstruction (Ma et al. 2020; Massey et al. 2018; Shao et al. 2021).

Many methods have been used for landslide hazard assessment in affected areas of an individual earthquake event, mainly including expert knowledge (Fall et al. 2006), Newmark model (Jibson et al. 2000), statistical analysis (Carrara et al. 1995) and Deep learning(Yang et al. 2022a, b; Yang et al. 2022a, b). The expert knowledge method established landslide assessment models based on limited information, and then rank and weight influencing factors based on professional knowledge (Anbalagan 1992; Msilimba and Holmes 2005). It should be noted that expert knowledge methods are usually applied in situations where the landslide data of the study area are scarce, or quantitative methods are not applicable. Otherwise, such methods heavily rely on the subjective knowledge of experts and often present significant subjectivity and error in the evaluation results (Van Westen et al. 1999). The Newmark method estimates seismic landslide displacement by simulating a landslide as a sliding block on an inclined plane with a known critical or yield acceleration (Newmark 1965). The modeled displacement serves as an indicator for assessing the seismic stability of the slope. However, utilizing the Newmark model for prediction necessitates precise input of the physical characteristics of rocks and ground motion parameters. Obtaining these parameters is often challenging given the existing technical limitations (Liu et al. 2017; Wang et al. 2021). As a result, assessing landslide hazards solely using the Newmark model remains full of challenges and risks (Chen et al. 2014; Ma and Xu 2019).

The landslide hazard assessment based on the statistical analysis method assumes that within a certain area, the influencing factors of past landslides will also lead to future. By analyzing the relationship between landslide influencing factors and the distribution of landslides that have already occurred, the landslide hazard assessment model can be established to conduct the potential landslide hazards assessment (Broeckx et al. 2018; Kritikos et al. 2015; Parker et al. 2017). Especially, with the development of GIS technology and machine learning, besides classical multivariate statistical methods including discriminant analysis and weight of evidence, more widely popular machine learning such as logistic regression (LR) models, support vector machines (SVM), random forests, and deep learning models have also been widely applied to landslide hazard assessment modeling (Kavzoglu et al. 2014; Merghadi et al. 2020; Sajadi et al. 2022; Shao and Xu 2022). Among them, the LR model is one of the most widely used models by virtue of its simplicity, high efficiency, and high prediction accuracy (Reichenbach et al. 2018). This method can carry out different types of independent variables including continuous variables and discrete variables, and the LR model can derive specific regression coefficients of independent variables. In recent years, few studies have focused on the establishment the earthquake-induced landslide hazard model at the national or global scale (Nowicki Jessee et al. 2019; Rosser et al. 2018; Shao et al. 2021). For example, Nowicki Jessee et al. (2019) established a new global model based on published 23 global coseismic landslide databases and LR modeling. This model can be applied to near real-time assessment of earthquake-induced landslides and medium to long-term hazard assessment in global regions. Wang et al. (2021) combined the Information value method with Newmark model to obtain the Chinese seismic landslide hazard assessment results. Xu et al. (2019) proposed a real probability prediction method for coseismic landslides by the Bayesian probability method and LR model and established a new generation of earthquake-triggered landslide hazard model in China based on nine earthquake cases. These studies have shown that the earthquake-induced landslide hazard assessment models for large-area scale, combined with probabilistic seismic hazard analysis can be used for conducting medium to long-term hazard assessment of earthquake-induced landslide hazards. Meanwhile, it is also the preferred method for establishing the near-real-time prediction model of earthquake-induced landslide hazards.

Aba Prefecture and Chengdu Plain region is located at the intersection of the eastern edge of the Qinghai-Tibet

Plateau and the South China Block. This area includes two geographical divisions: the west Sichuan Plateau mountainous area and the eastern Sichuan Basin. The Minjiang Fault and Huya Fault are distributed in a nearly north–south direction in the eastern boundary of the study area, as well as the Longmenshan fault with a northeast direction developed in the middle part of the area, which is an important component of China's famous north–south seismic zone (Hu et al. 2017; Wang et al. 2010). In recent years, several destructive earthquakes have occurred in Sichuan Province, such as the 2008 Ms8.0 Wenchuan earthquake (Xu et al. 2014), the 2013 Ms7.0 Lushan earthquake (Xu et al. 2015), the 2017 Ms7.0 Jiuzhaigou earthquake (Fan et al. 2018), 2022 Maerkang earthquake(Chen et al. 2023) and the 2022 Ms6.1 Lushan earthquake (Shao et al. 2022). These earthquake events triggered a large number of coseismic landslides, and also produced a large number of unstable and weakened slopes, further increasing the occurrence possibility of landslide disaster (Fan et al. 2019). Especially after the 2008 Wenchuan earthquake, massive post-quake landslides frequently occurred in the area and have obvious disaster-chain effects. Meanwhile, the post-quake landslide density increased by 1.55 times compared with the landslides before the earthquake. Influenced by frequent short-term heavy rainfall and human activities, the fragile geological environment has become more sensitive, and the scale and quantity of landsliding are much larger than before the earthquake. This phenomenon will last for a long time and cause serious harm to economic development and social stability (Fan et al. 2019; Xiong et al. 2021). Therefore, conducting a medium to long-term potential earthquake-induced landslide hazard assessment is crucial for emergency rescue and risk assessment of landslides in the Aba Prefecture and Chengdu Plain region.

Therefore, the purpose of this work is to carry out seismically induced landslide hazard mapping of Aba Prefecture and Chengdu Plain region. Based on nine earthquake-induced landslide databases around Aba Prefecture and Chengdu Plain region, this work can establish coseismic landslides evaluation model suitable for the study area based on the LR model. Based on the probabilistic seismic hazard analysis (PSHA), the distribution maps of predicted peak seismic motion under four earthquake occurrence scenarios are calculated. Using the distribution results of potential ground motion, the occurrence probability of earthquake-induced landslides in the study area under different ground motions is carried out. This study can provide important data support for the distribution pattern and potential hazard zoning of earthquake-induced landslides in southwestern China.

Geological and tectonic setting of the study area

Aba Prefecture and Chengdu Plain region are located in the northwest of Sichuan Province, with a longitude of 100°0′–104°7′E and a latitude of 30°5′–34°9′N. It is approximately 414 km long from north to south and 360 km wide from east to west, with a regional area of about 84,000 km^2. Structurally, it is located on the southeastern edge of the Qinghai Tibet Plateau at the intersection of the eastern edge of the Qinghai Tibet Plateau and the South China block. Affected by the Longmenshan Fault, Minjiang Fault and Huya Fault, this area is one of the high-hazard areas for earthquakes with high frequency and intensity in Sichuan Province (Fig. 1). In recent years, a series of destructive earthquakes have occurred in the region, such as the 2008 Wenchuan earthquake, the 2013 Lushan earthquake, and the 2017 Jiuzhaigou earthquake. The historical earthquakes data also show that most of the historical earthquakes in the entire Aba Prefecture and Chengdu Plain region are mainly distributed in the Longmenshan fault zone, Minjiang fault zone, and Huya fault zone, with 41 earthquakes with magnitudes between Ms6.0 and Ms7.0 and seven earthquakes with magnitude greater than Ms 7.0 (https://news.ceic.ac.cn/).

The terrain of the study area is higher in the northwest (Aba Prefecture) and lower in the southeast (Chengdu Plain), with a minimum elevation of 100 m and a maximum elevation of 7845 m. The area in the northwest has a continental plateau climate, which is mostly composed of high mountains and canyons with an average elevation of over 3500 m. The study area is cool in summer and cold in winter with an average annual temperature of only 0.8–4.3 °C and an average annual rainfall of 650 mm ~ 730 mm. The eastern area of the Sichuan basin has a subtropical humid climate with relatively low terrain, with most areas with elevations below 1000 m. The climate is mild and humid, with an average annual temperature of 8.3– 11.7 °C and an annual rainfall of 800 mm—910 mm. In addition, the study area has abundant water systems, with the Minjiang River and the largest tributary of the Dadu River crossing through the entire area. The area has abundant water resources and large natural waterfalls, which contain rich hydroelectric power resources (http://www.abazhou.gov.cn/abazhou/c104350/l_c.shtml).

Figure 2 illustrates the main strata exposed in the study area. The strata from the Cambrian (Є) to the Quaternary (Q) are distributed throughout the study area, of which the Jurassic (J) and Triassic (T) strata are the most widely distributed. Jurassic strata are mainly distributed in the southeast of the study area, and lithology mainly includes conglomerate, sandstone, siltstone and mudstone. The Triassic strata are mainly distributed in the northwest

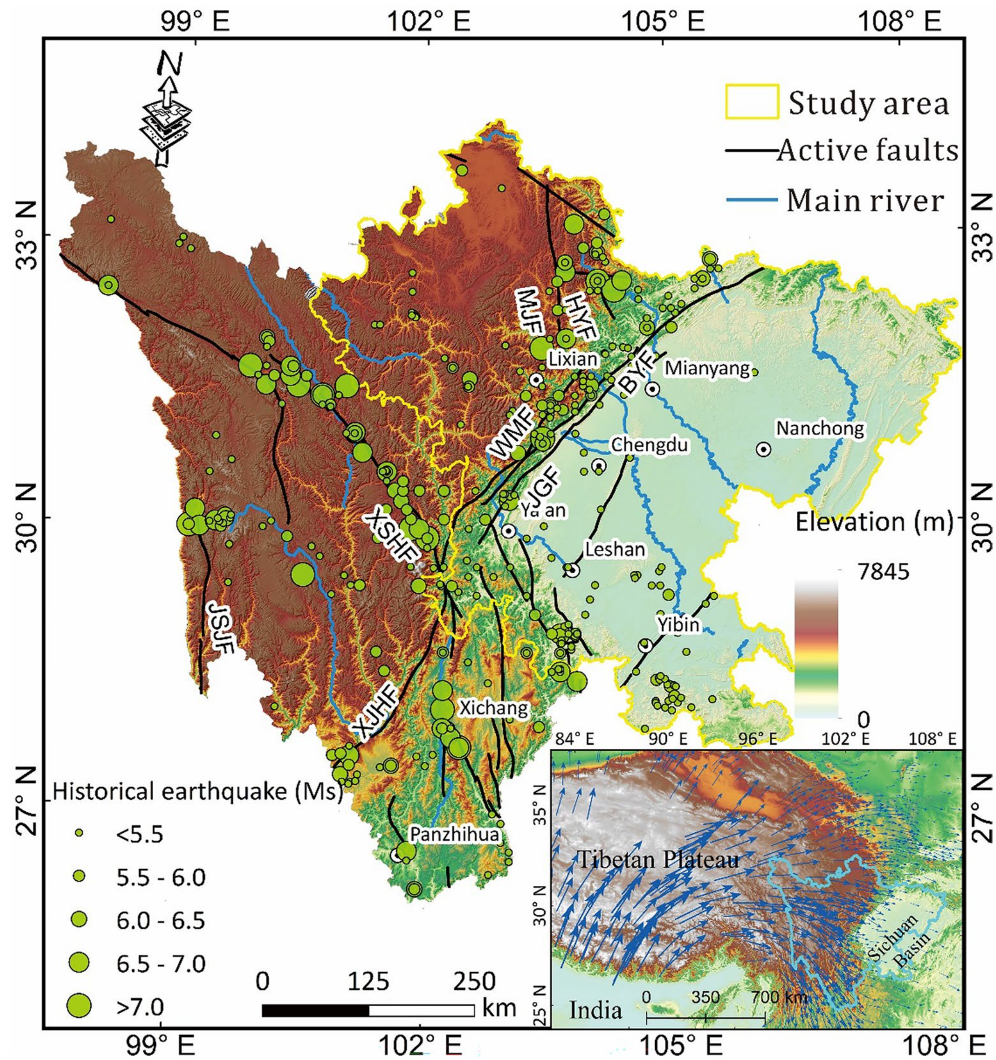

Fig. 1 Map showing the spatial distribution of active faults, historical earthquakes, and topographic features of the Sichuan Province. Longmenshan fault zone includes Wenchuan–Maoxian fault (WMF), Beichuan–Yingxiu fault (BYF) and Jiangyou–Guanxian fault (JGF); *XSHF* Xianshuihe fault, *HYF* Huya fault, *MJF* Minjiang fault, *XJHF* Xiaojinhe fault, *JSJF* Jinshajiang fault. The active fault lines are from Deng (2007). GPS data are from Zhao et al. (2015)

of the study area, and the lithology is mainly composed of sandstone, slate, and limestone. Meanwhile, the Cretaceous (K), Silurian (S), and Quaternary (Q) strata in the study area are also distributed. The Cretaceous strata are mainly distributed in the areas of Mianyang, Deyang, and Ya'an, with sandstone and mudstone. The Silurian (S) strata are mainly distributed in the northern part of the study area, with the lithology mainly consisting of medium to light metamorphic gray and green phyllite. Quaternary (Q) stratum is mainly composed of deposits from Early Pleistocene to early Holocene, mostly clay or sandy soil layer covered with gravel layer, mainly distributed in the interior of the basin. In addition, the igneous rock stratum in the study area is also widely developed, mainly distributed in the Pengguan complex between Yingxiu Beichuan fault and Wenchuan Maoxian fault, and the lithology is mainly granite and granodiorite. Under the strong influence of tectonics, the joint fissures in the rock mass study area are developed.

Materials and methods

Seismically induced landslides modeling

Similar terrain conditions and environment can trigger similar geological disasters when an earthquake occurs. This phenomenon is mainly related to the mechanism and influencing factors of earthquake geological disasters. The locations of previously triggered landslides provide crucial information about the geological

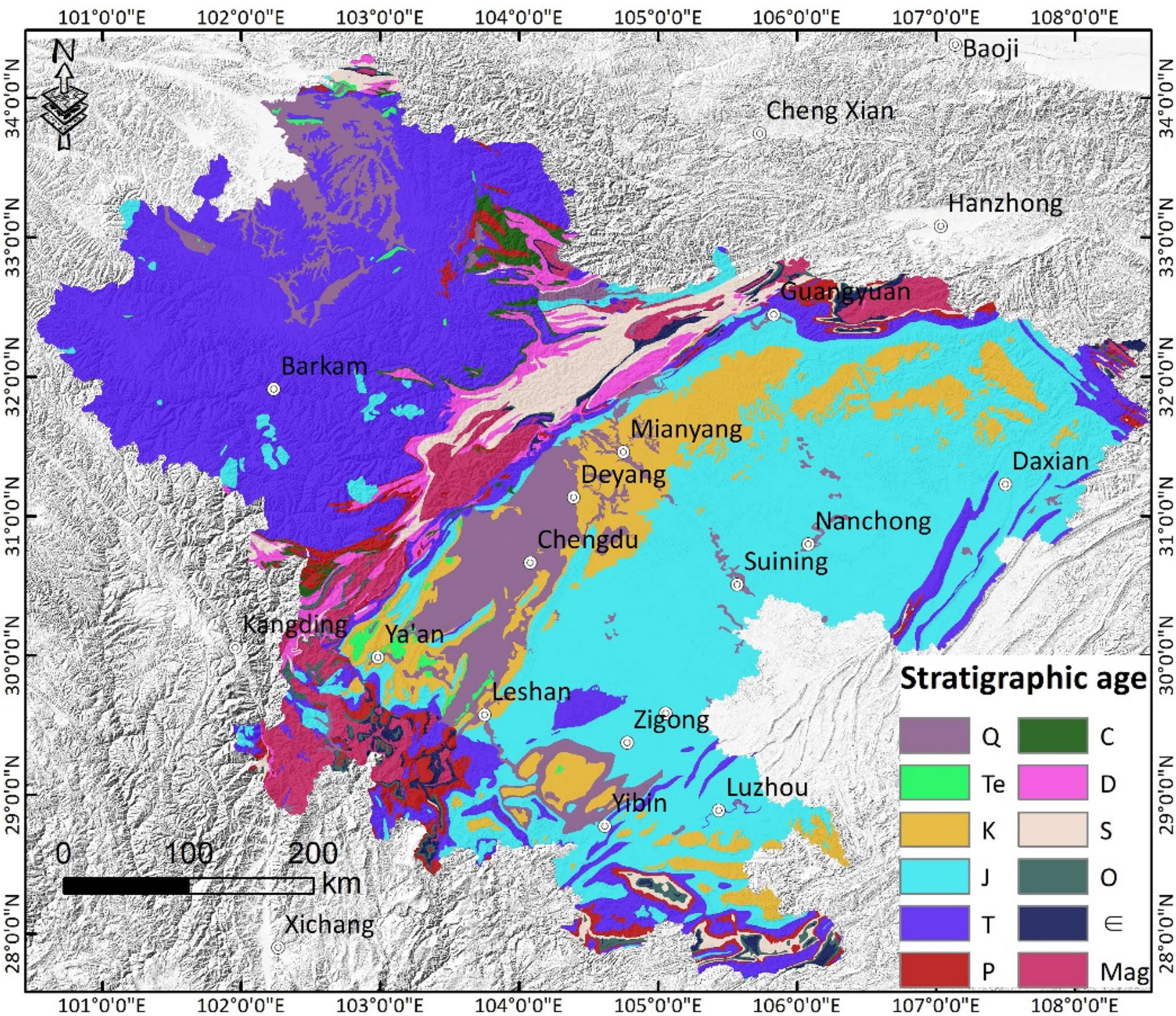

Fig. 2 Map showing the spatial distribution of the stratigraphic ages for the study area which was obtained from 1:200,000 geological maps published by the China Geological Survey (http://dcc.cgs.gov.cn/)

conditions in the area(Huang et al. 2022; Meunier et al. 2007). This includes soil types, geological features, slope steepness, orientation, and other factors closely related to landslide occurrences. Studying the geological conditions of triggered landslides can lead to a better understanding of the mechanisms behind landslide occurrences (Shao et al. 2023a, b). Therefore, when modeling, we try to select as many strong earthquake-triggered landslide databases within or around the evaluation area as possible as training samples. In this study, nine earthquake events that occurred in the study area and neighboring areas were selected, including the Ms 8.0 Wenchuan earthquake on May 12, 2008 (Xu et al. 2014), the Ms 7.1 Yushu earthquake on April 13, 2010 (Xu and Xu 2014), the Ms 7.0 Lushan earthquake on April 20, 2013 (Xu et al. 2015), the Ms 6.6 Minxian earthquake on July 21, 2013(Tian et al. 2016), the Ms 6.5 Ludian earthquake on August 3, 2014 (Wu et al. 2020), the Ms 7.0 Jiuzhaigou earthquake on August 8, 2017(Tian et al. 2019), the Ms6.9 Milin earthquake on November 17, 2017(Huang et al. 2021a, b), the Ms 5.7 Xingwen earthquake on December 16, 2018 (Huang and Xu 2020), and the Ms6.0 Changning earthquake on June 17, 2019 (Huang et al. 2021a, b). For all the available inventories, landslides have been mapped as polygons from aerial photographs and satellite imagery, as well as conducting field surveys. Nine earthquakes include a total of 251260 landslides, with the Wenchuan earthquake triggering the most, with 197,481 landslide records. More information on earthquake and landslides data related to nine earthquake events can be found in Table 1.

According to the Bayesian probability theory, the occurrence probability of the coseismic landslides for a single earthquake event is the ratio of the total landslide area to the area of the entire study area, that is, the prior probability of the occurrence of the coseismic landslide of the earthquake event (Shao et al. 2020, 2021). Based on the distribution characteristics of the nine quake events, the coseismic landslides of the nine events are distributed in areas with intensities of VI or above. Therefore, we randomly generated sample points in the study area. Based on a previous study (Shao et al. 2020), the sampling intensity is 200 grid cells/ km^2. The points falling within the landslides area were sliding samples, and the rest were non-sliding samples. This ensured that the ratio of the sliding to the non-sliding was equivalent to the occurrence probability of the coseismic landslides in the study area.

Currently, the logistic regression (LR) model is the preferred method for evaluating earthquake-induced landslide hazards (Nowicki Jessee et al. 2019; Tanyas et al. 2019). This model can model different types of independent variables (including continuous and discrete variables) and does not require any assumptions about the distribution of the identifying variables. Based on the regression coefficients of the various influencing factors in the LR model, the predicted probability can be obtained by superimposing the layers of the various influencing factors. The LR model converts the dependent variable into a binary logical variable that either occurs (represented by 1) or does not occur (represented by 0). The relationship between the probability of landslide occurrence and the influencing factors can be expressed as:

$$Z = \beta_0 + \beta_1\chi_1 + \beta_2\chi_2 + \beta_3\chi_3 \ldots \beta_i\chi_i \quad (1)$$

$$P = 1/\left(1 + e^{-z}\right), \quad (2)$$

where P represents the probability of landslide occurrence, ranging from [0,1]. Z represents the sum of linear weight values after variable superposition; χ_i represents various influencing factors, β_i is the logistic regression coefficient.

Influencing factors data

Earthquake-induced landslides are mainly affected by the combination of different influencing factors, such as seismic motion, topography, geology, hydrology, etc. (Ling et al. 2020; Watkinson and Hall 2019; Zhao et al. 2022). In this study, 12 factors were selected, including elevation, slope, aspect, relief, topographic wetness index (TWI), topographic position index (TPI), peak ground motion, distance to active faults, vegetation coverage, distance to roads, lithology, and annual rainfall to establish the LR model (Figs. 2, 3). Elevation can influence the distribution of water flow, soil stability, and overall terrain characteristics. Higher elevation areas might experience increased soil erosion due to runoff, potentially leading to landslides. Steeper slopes are more prone to gravitational forces and erosion, making them susceptible to landslides(Saleem et al. 2019). Slope angle directly affects the stability of the terrain. Different aspects can lead to variations in soil properties and vegetation growth, affecting landslide susceptibility (Cellek 2021). Higher relief areas may experience more significant water drainage, increasing the potential for landslides. TWI quantifies the tendency of an area to accumulate water. High TWI values indicate areas prone to water saturation, which can reduce soil cohesion and increase landslide risk. TPI identifies whether a point is situated in a ridge, slope, or valley. It helps capture local topographic features that influence water accumulation and soil stability. Peak ground motion, caused by seismic activity or human activities, can trigger landslides (Pourghasemi et al. 2018). High peak ground motion areas are more

Table 1 List of the coseismic landslide inventories of nine earthquake events used in this study

No.	Date	Location	Magnitude (Ms)	Focal depth (km)	Maximum intensity	Epicenter location	Number of landslides	Total landslide area (km^2)	Affected area (km^2)
1	2008/05/12	Wenchuan earthquake	8.0	19	IX	31.002°N, 103.322°E	197,481	1159.9	75,481
2	2010/04/13	Yushu earthquake	7.1	17	IX	33.165°N, 96.548°E	2036	1.2	1455
3	2013/04/20	Lushan earthquake	7.0	14	VII	30.308°N, 102.888°E	22,528	18.9	4949.8
4	2013/07/21	Minxian earthquake	6.6	8	VII	34.512°N, 104.262°E	6479	1.8	830.2
5	2014/08/03	Ludian earthquake	6.5	12	VIII	27.189°N, 103.409°E	12,817	16.3	600
6	2017/08/08	Jiuzhaigou earthquake	7.0	9	VII	33.193°N, 103.855°E	4834	9.6	284.3
7	2017/11/17	Milin earthquake	6.9	10	VIII	29.75°N, 95.02°E	3130	4.35	2360
8	2018/12/16	Xingwen earthquake	7.9	12	VII	28.24°N, 104.95°E	288	0.49	600
9	2019/6/17	Changning earthquake	6.0	16	VIII	28.34°N, 104.90°E	496	1.2	300

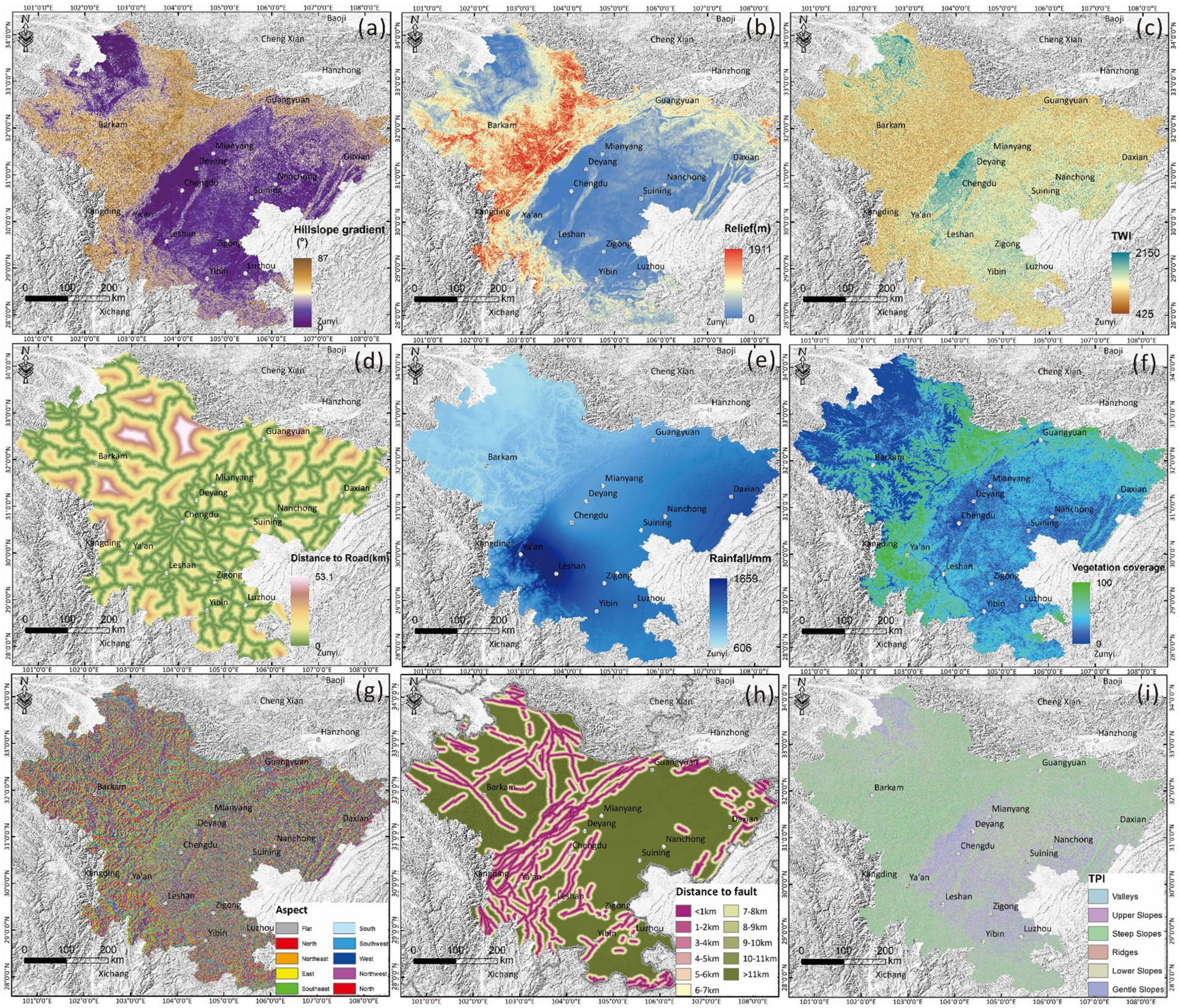

Fig. 3 Map showing the spatial distribution of relevant influencing factors for LR modeling: **a** slope angles; **b** topographic relief; **c** topographic wetness index (TWI); **d** distance to roads; **e** annual rainfall; **f** vegetation coverage; **g** slope aspect; **h** distances to active faults; **i** TPI (topographic position index)

likely to experience slope instability during an earthquake. Proximity to active faults indicates tectonic activity, which can cause ground shaking and displacement, leading to landslides. Vegetation stabilizes soil by reducing erosion, enhancing root cohesion, and absorbing excess water. Sparse vegetation can weaken the soil's stability and increase landslide susceptibility. Road construction and human activities near roads can alter drainage patterns and soil stability. Areas close to roads might experience increased disturbance and erosion, elevating landslide risk (Shao and Xu 2022). Different rock types have varying strengths and weathering rates. Weaker lithologies are more susceptible to erosion and may lead to landslides. Rainfall, particularly heavy and prolonged rainfall, is a major trigger for landslides. Excessive water can saturate the soil, reducing friction and triggering slope failures(Vorpahl et al. 2012).

The ALOS DEM data with a resolution of 25 m were used to obtain the elevation information of the study area (https://www.eorc.jaxa.jp/ALOS/en/aw3d30/index.htm). The DEM data were used to calculate the hillslope gradient and slope aspect(Fig. 3a, g). We also calculated the topographic relief based on the elevation range within a 1.0 km radius (Fig. 3b). TWI was calculated by GRASS GIS and elevation data, and drainages were derived using ArcGIS from the DEM (Fig. 3c). The vegetation coverage of the study area is set at 0–100%, and the vegetation coverage of the body of water is assigned a value of

-1 (http://www.iscgm.org/) (Tateishi et al. 2011) (Fig. 3f). The active fault data adopt the national seismotectonic map (Xu et al. 2016). According to the interval of 1 km, the study is divided into 11 categories, namely, 0 ~ 1 km, 1 ~ 2 km, 2 ~ 3 km, 3 ~ 4 km, 4 ~ 5 km, 5 ~ 6 km, 6 ~ 7 km, 7 ~ 8 km, 8 ~ 9 km, 9 ~ 10 km and > 10 km from the active faults (Fig. 3h). Stratigraphic data are from the 1: 250,000 geological map of China published by the China Geological Survey (http://dcc.cgs.gov.cn/). According to the geological age, the stratigraphy of the study area is divided into 12 categories, from new to old, namely the Quaternary (Q), Tertiary (Te), Cretaceous (K), Jurassic (J), Triassic (Tr), Permian (P), Carboniferous (C), Devonian (D), Silurian (S), Ordovician (O), Cambrian (∈), and Precambrian (Pre∈). The annual average rainfall data are from the global rainfall data, with a resolution of about 1 km(Fick and Hijmans 2017). The annual average rainfall map of the study area with a resolution of 25 m is produced by using the linear interpolation method to match the resolution of other influencing factors (Fig. 3e). The peak ground motion acceleration (PGA) comes from PGA distribution map published by the United States Geological Survey (USGS) which is calculated by combining actual station data and numerical simulation of each earthquake. Based on the information related to seismic motion distribution published by USGS, the PGA information of each earthquake event can be obtained.

Probabilistic seismic hazard analysis

Cornell (1968) established the probabilistic of seismic hazard and analysis (PSHA) based on the Poisson distribution model, and this method has become the most commonly used method for seismic hazard analysis worldwide (Ahulu et al. 2018; Sana 2019). Considering the characteristics of spatiotemporal heterogeneity of earthquakes within the Chinese Mainland, the probabilistic seismic hazard analysis method considering spatiotemporal heterogeneity of seismicity was proposed (Hu 2002). In recent years, some studies have proposed methods for the three-level division of potential source areas, clarifying the impact of block action boundaries on the determination of the range of potential source areas and the upper limit of earthquake magnitudes. This method used paleoseismic data, seismic data, fault activity rate, GPS data to determine the recurrence period and annual average occurrence rate of high-magnitude earthquakes, the Seismic Ground Motion Parameter Zoning Map of China was prepared by the new near site seismic attenuation relationship of large earthquakes and the seismic ground motion attenuation relationship of moderately strong seismicity areas (Gao 2021). However, this method only considers the seismic hazard caused by fault segmentation or historical earthquake rupture segmentation and does not consider the occurrence rate of major cascading-rupture earthquakes that may exceed the historical maximum magnitude.

The 2008 Wenchuan earthquake belongs to the cascade rupture type earthquake, which is completely different from the prediction results based on historical earthquake rupture segmentation in existing earthquake risk prediction models. For specific strike slip-fault parts, long-term earthquake risk assessment based on cascade rupture segments tends to be more reasonable (Wen 2001). Meanwhile, it is of great practical significance to consider the occurrence rate of catastrophic cascading fractures in the new seismic risk model (Cheng et al. 2020). Active faults are the main locations where earthquakes occur in the entire seismic source area, and major earthquakes generally occur on major active faults. The length of the rupture increases with the magnitude of the earthquake. Cheng et al. (2020) used the Tapered Gutenberg–Richter relationship (TGR) (Kagan 2002) instead of the truncated G-R relationship to control the maximum earthquake in the source zone in the Global Earthquake Model (GEM) OpenQuake tool (Silva et al. 2020, 2014). Based on the original values of a and b in the G-R relationship, the revised model added the unknown quantity of MC (corner magnitude) to control curve change to obtain the occurrence rate of major earthquakes by formulas (3) and (4)):

$$\mathrm{F(M)} = \alpha_t \left(\frac{M_t}{M}\right)^{\beta} exp\left(\frac{M_t - M}{M_c}\right)(M_t \leq M \leq \infty). \tag{3}$$

The unit of M is N.m, F(M) is the earthquake occurrence rate of seismic moment greater than, β=2b/3, M_t is the seismic moment of the smallest earthquake in the integrity catalog, and α_t is the earthquake occurrence rate corresponding to the earthquake of seismic moment greater than or equal to M_t. M_c can be estimated by the conservation criterion of seismic moment:

$$\mathrm{M}_c = [\frac{\chi \dot{M_{T0}}(1-\beta)}{\alpha_t M_t^{\beta}\Gamma(2-\beta)}]^{1/(1-\beta)}. \tag{4}$$

M_c is the total seismic moment accumulation rate given by geodesy or geological survey. χ is the seismic release coupling factor of this accumulation rate, and Γ is the gamma distribution equation. M_{T0} can be estimated using strain rate models derived from geodetic data.

$$\dot{M_{T0}} = \mathrm{A(cz)}\begin{cases} \dot{2}_3;\ (\dot{2} < 0) \\ -\dot{2}_1;\ (\dot{2} \geq 0), \end{cases} \tag{5}$$

where A is the grid area, c is the coupling degree, z is the depth of the seismogenic layer in km, and (cz) is the average coupled depth of the seismogenic layer.

Cheng et al. (2020) established a seismic risk prediction model for the Sichuan Yunnan region considering major earthquakes exceeding the historical maximum magnitude, and use OpenQuake to calculate the PGA distribution in the Sichuan Yunnan region. In this study, we combined the above model to calculate the PGA distribution in the study area under different earthquake scenarios including frequent, occasional, rare, and very rare earthquake occurrence.

Results and analysis

In this study, we calculated the distribution of peak ground acceleration (PGA) under four earthquake scenarios, including frequent, occasional, rare, and very rare earthquake occurrence. These four earthquake scenarios correspond to the seismic motion distribution under different exceedance probabilities. Figure 4 shows the spatial distribution of PGA under different exceedance probability conditions. Overall, the PGA in the eastern region is significantly lower than that in the western region, and as the probability of exceedance increases, the corresponding PGA also gradually decreases. From the overall distribution of the predicted PGA results for four earthquake scenarios, it can be seen that active faults have a significant effect on the spatial distribution of PGA, and the high-value areas of PGA are roughly located near the active faults, such as the middle section of the Longmenshan fault zone and the both sides of the Huya fault

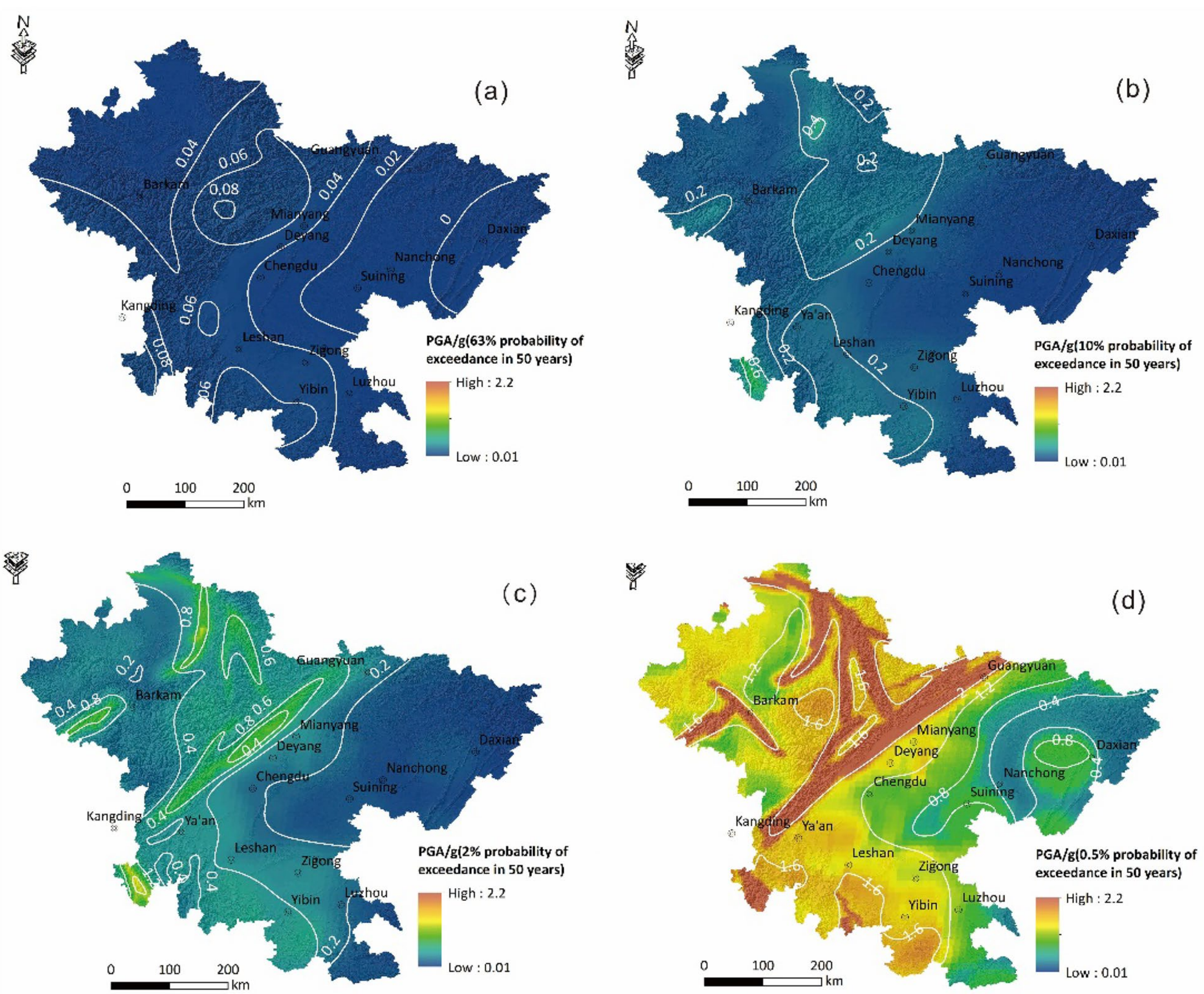

Fig. 4 Map showing the PGA distribution of the study area under four earthquake scenarios: **a** PGA distribution with a probability of exceeding 63% in 50 years for frequent earthquake occurrence; **b** PGA distribution with a probability of exceeding 10% in 50 years for occasional earthquake occurrence; **c** PGA distribution with a probability of exceeding 2% in 50 years for rare earthquake occurrence; **d** PGA distribution with a probability of exceeding 0.5% in 50 years for very rare earthquake occurrence

and the Minjiang fault zone. For extremely rare and rare earthquake scenarios, PGA is significantly controlled by active faults. Most areas with high PGA values (i.e., red areas) are mainly distributed within a 25 km range on both sides of the Longmenshan and Minjiang fault zones. The maximum PGA values calculated for extremely rare and rare earthquake scenarios reach 2.13 g and 1.37 g, respectively (Fig. 4d, c). For the occasional earthquake scenario, we can see that the control of Longmenshan fault zone on ground motion is significantly reduced. The areas with high PGA values are located in the Northwest and Southwest areas of the Sichuan basin, and the area with the largest PGA value of 0.8 g appears in the west of Minjiang fault (Fig. 4b). For frequent earthquake scenarios, we can observe that the PGA values in most areas are generally below 0.05 g, while the areas with high PGA are generally located in the northwest region of the Longmenshan Fault zone, with a maximum PGA value of 0.09 g of Kangding are also potential high-hazard areas (Fig. 4a).

According to the regression coefficients, the relationship between each influencing factor and landslide occurrence can be analyzed. For continuous variables, a positive sign indicates that the explanatory variable has increased the probability of change, and a negative sign implies the opposite effect. The regression coefficient for elevation is -0.00034, indicating that earthquake-induced landslides often occur in areas with lower elevations. This may be because areas with lower elevations accumulate more loose deposits, which have a loose structure and are more prone to landslides under strong ground motion. The regression coefficient for slope angle is 0.026535, indicating a positive correlation between coseismic landslides and slope gradient. The higher the slope gradient, the higher the probability of landslide occurrence. The regression coefficient for topographic relief is 0.002227, indicating a positive correlation between the probability of earthquake-induced landslides and relief. Generally, the areas with higher topographic relief have steep terrain and are more prone to landsliding. In addition, there is a positive correlation between average rainfall and earthquake-induced landslides, with a regression coefficient of 0.001484. The regression coefficient for vegetation coverage is − 0.01132, indicating a negative correlation between vegetation coverage and earthquake-induced landslides. The greater the vegetation coverage, the less likely coseismic landslides are to occur. The regression coefficient for distance to roads is − 1.16977, indicating a negative correlation between distance to roads and earthquake-induced landslide occurrence. The farther away from roads, the less likely landslides are to occur.

For the categorical variable, the weight of each classification within the influencing factor is significantly different, which indicates that different classifications have distinct effects on the coseismic landslide. Figure 5 is the regression coefficient of four categorical variables (slope aspect, fault distance, TPI, and strata of different ages) in different classification intervals. Figure 5a shows the regression coefficients corresponding to different aspects. Overall, the regression coefficients for the east aspect are larger than those for the west aspect, which may indicate that the east slope is more prone to landslides. Among them, the regression coefficients for the northeast and East slopes are the highest, with values of 0.18 and 0.16, respectively. Figure 5b shows the regression coefficients for distance to faults. The results show that the overall regression coefficient gradually decreases with the increase of distance to faults, indicating a significant negative correlation between distance to fault and landslides. The further away from the fault, the less likely it is that landslides will occur. Figure 5c shows the regression coefficients corresponding to Topographic Position Index (TPI). The results show that the regression coefficients for gentle slopes are the lowest, while the regression coefficients for valleys and ridge areas are the highest, indicating a greater likelihood of earthquake-induced landslides occurring in valleys and ridge areas. Figure 5d is the regression coefficient corresponding to strata of different ages. The statistical results show that the stratum with the largest regression coefficient is the magmatic rock stratum, which is mainly because the magmatic rock stratum in the study area is mainly distributed in the Pengguan complex rock mass between Yingxiu–Beichuan fault and Wenchuan–Maoxian fault. Due to the strong influence of tectonics, the joint fissures of the rock mass are very developed, resulting in a significant reduction of the actual rock mass strength relative to the rock mass, Therefore, this area is more prone to landslides under the action of strong ground motion.

Based on the trained LR model, we can calculate the occurrence probability of earthquake-induced landslides in the study area under four future earthquake scenarios, including frequent earthquake occurrence with a probability of exceeding 63% in 50 years, occasional earthquake occurrence with a probability of exceeding 10% in 50 years, rare earthquake occurrence with a probability of exceeding 2% in 50 years and very rare earthquake occurrence with a probability of exceeding 0.5% in 50 years. Using the PGA distribution of the four scenarios as input data, we calculated the occurrence probability of seismic landslides in the study area under the action of different peak ground motions. The results show that the high-hazard areas are mainly concentrated in the Longmenshan fault zone, and the southern area of Kangding is also a potential high-hazard area for landsliding. Meanwhile, as the probability of exceedance decreases, the

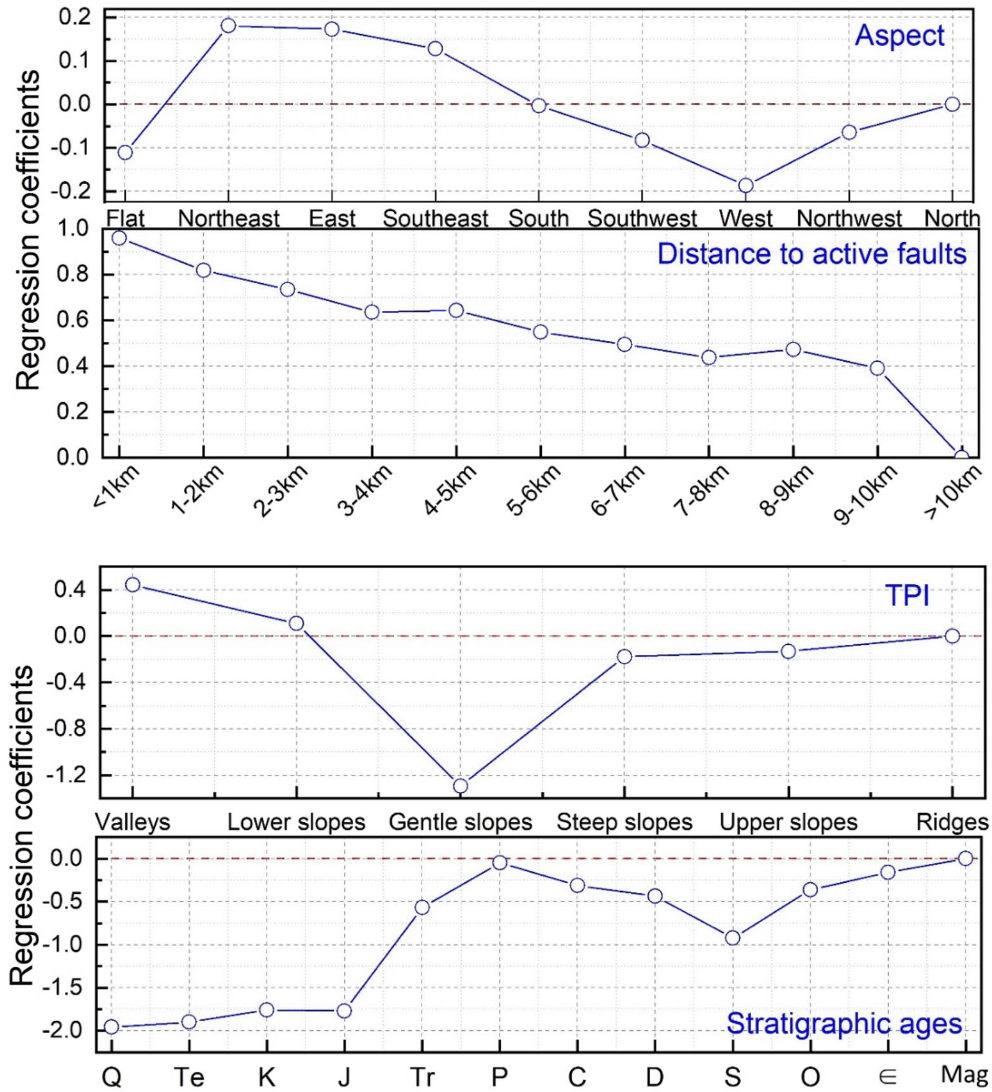

Fig. 5 Map showing regression coefficient of different classification attributes of four categorical variables in LR model modeling: **a** aspect; **b** distance to active faults; **c** topographic position index (TPI); **d** stratigraphic ages

probability of corresponding earthquake-induced landslides and the area of high-hazard regions also significantly increase. For the frequent earthquake scenario, the predicted probability of landslide occurrence is mainly concentrated in the northern area of the Longmenshan fault zone, especially in the Pengguan complex rock mass near the epicenter of the 2008 Wenchuan earthquake, which is the landslide abundance area during the earthquake. In addition, the high mountainous and canyon areas in the south of Kangding are also potential high-hazard areas (Fig. 6a). For the occasional earthquake scenario, the potential high-hazard areas for earthquake-induced landslides are roughly the same as those for the frequent earthquake scenario, mainly located in the northern part of the Longmenshan fault zone and the southern part of the Kangding area. However, the predicted probability of a landslide is significantly higher, with the maximum value being 0.44 (Fig. 6b). For the rare earthquake scenario, we can observe that the predicted area of high-hazard significantly increased, the areas near the Minjiang fault zone and the southern area of Ya'an are predicted as potential high-hazard areas of coseismic landslides. Otherwise, the southern area of the Longmenshan fault zone is also predicted as a high-hazard area for landslides with the PGA value increases (Fig. 6c). For the extremely rare earthquake occurrence scenario, we can observe that almost the entire Longmenshan area is located in potential high-hazard areas for coseismic

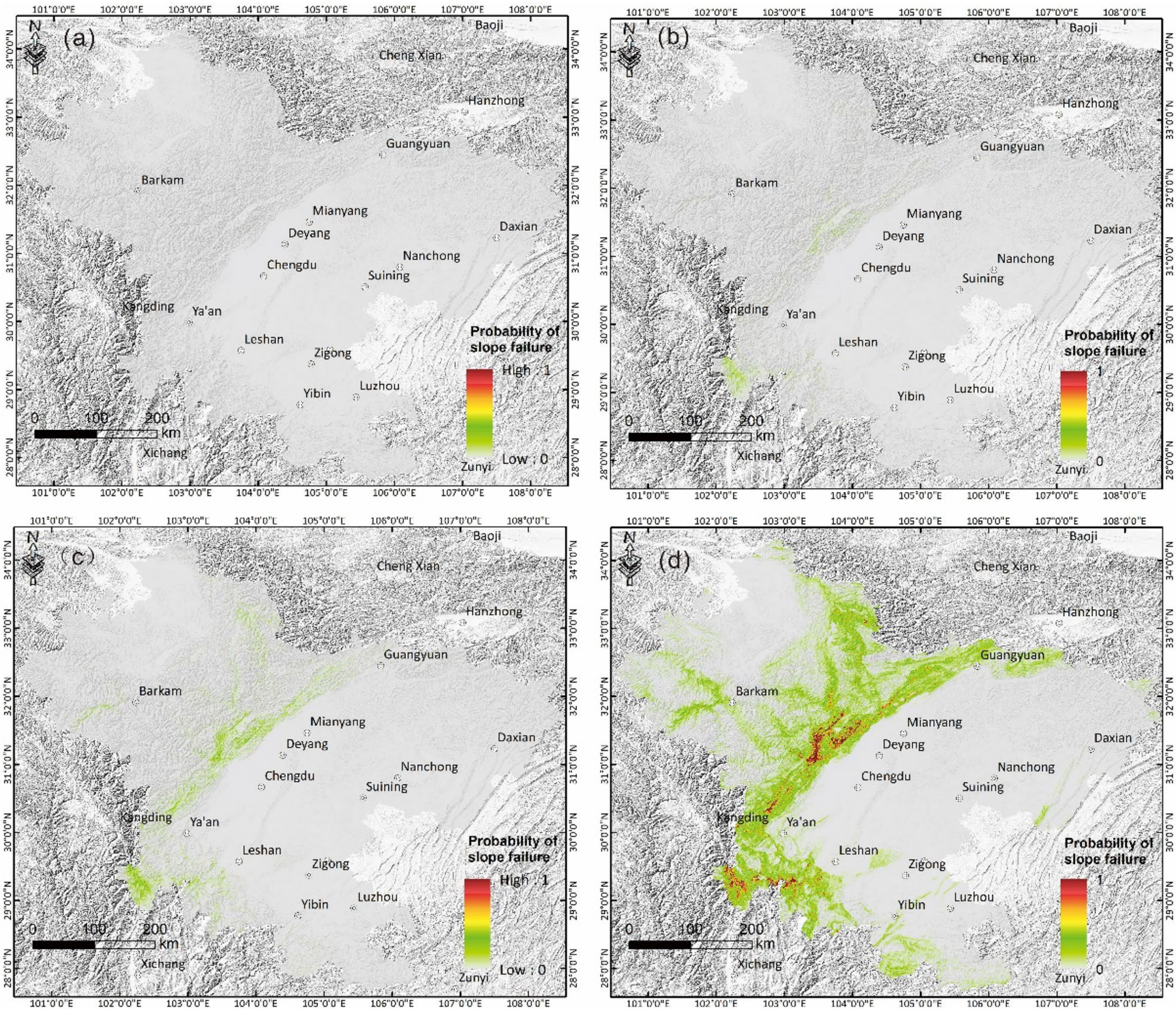

Fig. 6 Map showing the predicted occurrence probability of coseismic landslide under four earthquake occurrence scenarios: **a** PGA distribution with a probability of exceeding 63% in 50 years for frequent earthquake occurrence; **b** PGA distribution with a probability of exceeding 10% in 50 years for occasional earthquake occurrence; **c** PGA distribution with a probability of exceeding 2% in 50 years for rare earthquake occurrence; **d** PGA distribution with a probability of exceeding 0.5% in 50 years for very rare earthquake occurrence

landslides, while surrounding regions of other active faults, including the southern section of the Minjiang and Xianshuihe fault zones, are also high-hazard areas for coseismic landslides (Fig. 6d).

Based on previous studies (Shao et al. 2021; Xu et al. 2019), the predicted occurrence probability of coseismic landslide is divided into extremely low hazard areas (0–0.001%), low hazard areas (0.001– 0.01%), medium hazard areas (0.01 – 0.1%), high hazard areas (0.1–1%), and extremely high hazard areas (> 1%). Figure 7 shows landslide hazard maps under four seismic motion scenarios. The results show that the high and extremely high hazard areas of the study area are mainly concentrated in the vicinity of the main active fault zones, especially in the Longmenshan fault zone. Meanwhile, as the probability of exceedance decreases, the area of potential high-hazard areas for earthquake-induced landslides rapidly decreases. For frequent and occasional earthquake scenarios, the high-hazard areas are mainly distributed in the northern part of the Longmenshan fault zone (Fig. 7a, b). For rare and extremely rare earthquake scenarios, the area of extremely high hazard in the study area has significantly increased (Fig. 7c, d). For rare earthquake occurrence scenarios, the entire southern part of the Longmenshan fault, Minjiang fault, and Xianshuihe fault zone is roughly classified as extremely high-hazard areas.

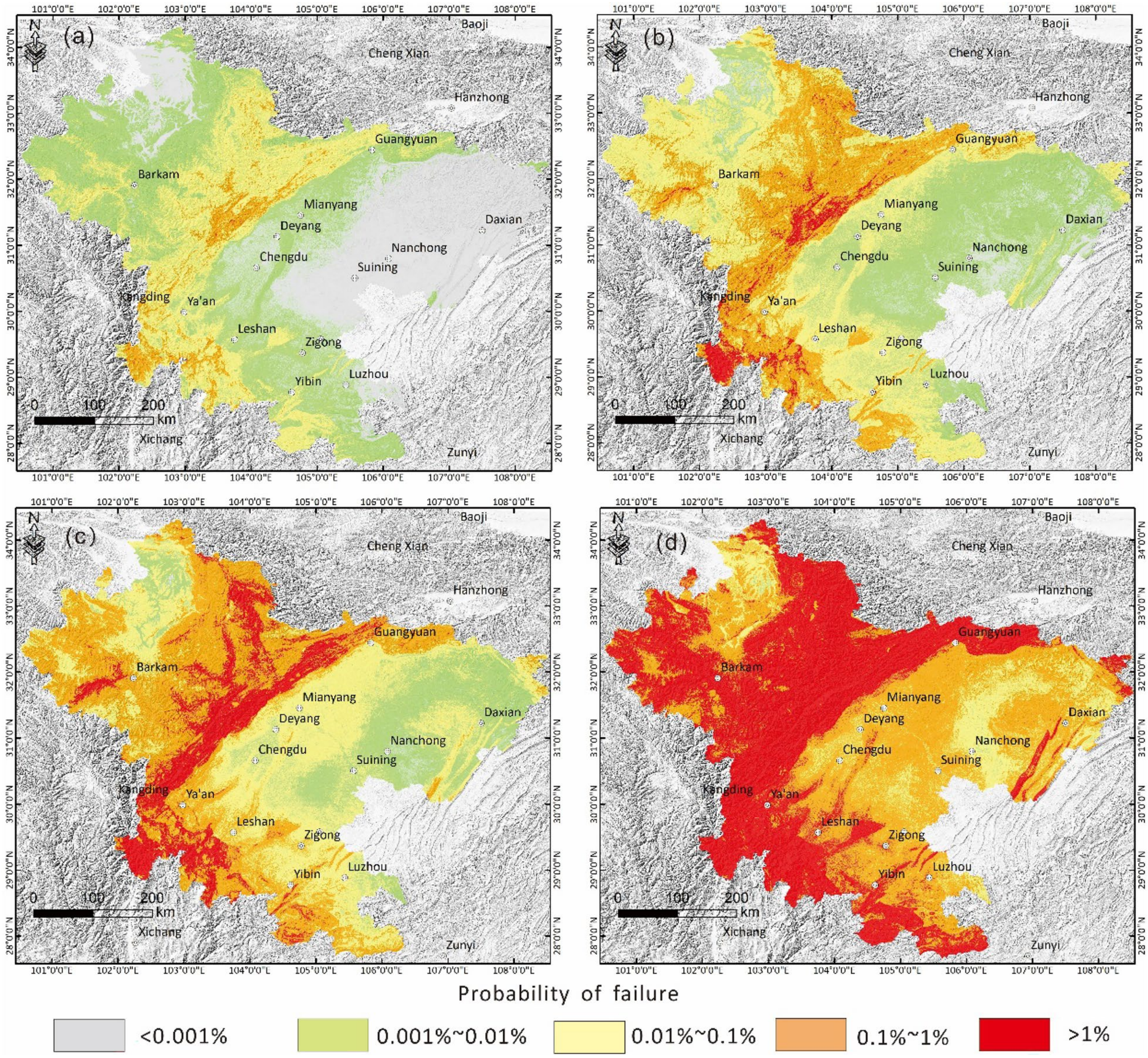

Fig. 7 Landslide hazard map under four earthquake occurrence scenarios: **a** PGA distribution with a probability of exceeding 63% in 50 years for frequent earthquake occurrence; **b** PGA distribution with a probability of exceeding 10% in 50 years for occasional earthquake occurrence; **c** PGA distribution with a probability of exceeding 2% in 50 years for rare earthquake occurrence; **d** PGA distribution with a probability of exceeding 0.5% in 50 years for very rare earthquake occurrence

For extremely rare earthquake scenarios, except for the Sichuan basin, other regions are roughly classified as extremely high-hazard areas.

The statistical results for each hazard classification of the four scenarios of earthquake occurrence indicate that as the probability of exceedance decreases, the corresponding predicted high and very high hazard area of coseismic landslides increases (Fig. 8). For the frequent earthquake occurrence scenario, the area of the extremely high-hazard zone is about 89 km^2, accounting for 0.03% of the total study area, with the landslide area density (LAD) of 1.28%. The area of extremely low-hazard zones is about 67,000 km^2, accounting for 26.2% of the total study area, with the LAD of 0.0004%. For the occasional earthquake scenario, the area of the extremely high-hazard zone is 8,600 km^2, accounting for 3% of the total study area, with the corresponding LAD of 2.55%. The area of extremely low-hazard zones is 12,900 km2, accounting for 5.1% of the total study area, with a LAD of 0.0006%. For the rare earthquake scenario, the area of extremely high-hazard zones is about 33,300 km^2, accounting for 13% of the total study area, with a LAD

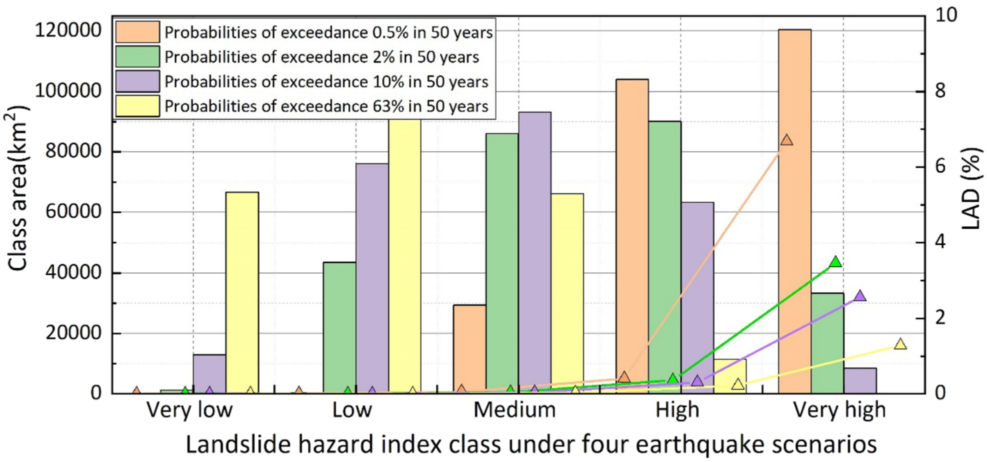

Fig. 8 Histogram showing class area and landslide areal density (LAD) for different landslide hazard index classes under four earthquake occurrence scenarios

of 3.46%. The area of extremely low-hazard zones is 1260 km^2, accounting for 0.49% of the total study area, with a LAD of 0.0007%. For the extremely rare earthquake occurrence scenario, the area of extremely high-hazard zones is 120,500 km^2, accounting for 47% of the total study area, with a landslide density of 6.7%.

Discussion

In recent years, a large number of achievements have emerged in the construction of near real-time coseismic landslide hazard assessment models based on massive landslide data (Cao et al. 2019; Nowicki Jessee et al. 2019; Tanyas et al. 2019). However, most of these models are trained based on global coseismic landslide databases (Nowicki Jessee et al. 2019; Nowicki et al. 2014; Tanyas et al. 2019). Therefore, due to the different terrain, geological, and tectonic conditions, the applicability of hazard assessment models based on global coseismic landslide databases may not be applicable in an individual earthquake event (Allstadt et al. 2018). In this study, in order to construct an earthquake-induced landslide assessment model suitable for the study area, nine earthquake events that occurred in the study area and neighboring areas were selected. These landslide databases provide us with abundant training samples for constructing earthquake-induced landslide evaluation models. More than 250,000 actual landslide recordings are included in the LR modeling, with more than 70% of those records coming from the 2008 Ms8.0 Wenchuan earthquake. The Wenchuan event caused massive landslides, and since this earthquake continues to dominate the global data set, the landslide samples from the Wenchuan events have the greatest influence on the construction of the LR model, which results in the highest applicability and accuracy of the model in the Wenchuan region. The same phenomenon can also be found in previous studies (Nowicki Jessee et al. 2019; Nowicki et al. 2014).

After an earthquake occurs, time is life. By utilizing geological and terrain data of quake-affected areas, we can carry out rapid assessment and quickly identify high-hazard areas of coseismic landslides combined with near-time peak ground motion distribution, which can provide a basis for optimizing emergency deployment of quake-affected areas (Ma et al. 2020; Robinson et al. 2017). In this study, we established a coseismic landslide hazard assessment model suitable for Sichuan Province based on nine earthquake events that occurred in Aba Prefecture and Chengdu Plain region and neighboring areas. Using this model, we can calculate the occurrence probability of earthquake-induced landslides based on the PGA distribution. Furthermore, we can conduct medium to long-term probabilistic assessments of earthquake-induced landslide hazards. This assessment is focused on specific earthquake scenarios that might occur in the future. The primary goal of this approach is to enhance our ability to provide effective emergency response and implement medium to long-term strategies for mitigating the impact of earthquake-induced landslides. Meanwhile, in subsequent studies, we can also conduct post-quake hazard and risk assessments based on rainfall data and strong aftershocks, and relevant hazard and risk assessments of landslides after earthquakes by overlaying population and economic data, providing data support for post-quake recovery and reconstruction phase.

At present, due to scale limitations and computational efficiency, the resolution of basic input data for earthquake-induced landslide hazard assessment models ranges from 100 to 1000 m (Nowicki Jessee et al. 2019;

Xu et al. 2019), which to some extent affects the prediction accuracy of the modeling, resulting in errors of at the local scale (Allstadt et al. 2018). Therefore, in this study, we chose ALOS DEM data with a resolution of 25 m for LR modeling, thereby ensuring the accuracy of the predictive ability of the assessment model. In addition, we selected 13 commonly used influencing factors for establishing the coseismic landslide hazard assessment model. These 13 influencing factors include the potential factors that may affect the occurrence of landslides. However, due to the large scale of the study area and the large number of training samples, we have not carried out relevant studies on the impact of different training samples and combinations of different influencing factors on the prediction results, which may cause some influencing factors to have a certain collinearity, thus increasing the complexity of the model and reducing the prediction ability (Nowicki Jessee et al. 2019; Xu et al. 2019). Meanwhile, it should be pointed out that there may be potential influencing factors, such as slope type, ground deformation of an earthquake, and properties of seismogenic fault, which may be potential factors affecting cosiesmic landslide occurrence. Therefore, in order to construct models with better predictive ability. We will further conduct a quantitative analysis of different combinations of influencing factors on model construction in future work.

Conclusions

Our study has conducted a comprehensive assessment of coseismic landslide hazards in the Aba Prefecture and Chengdu Plain region, utilizing data from nine earthquake events and a total of 251,260 landslide records. Employing probabilistic seismic hazard analysis (PSHA), we assessed the distribution of seismic peak ground motion predictions under four distinct earthquake occurrence scenarios, ranging from frequent to very rare earthquake occurrence.

Our findings reveal significant regional variations in peak ground acceleration (PGA), with the eastern region exhibiting notably lower values compared to the western region. Furthermore, as the probability of exceedance increases, there is a corresponding gradual decrease in PGA. Specifically, for rare and very rare earthquake occurrence scenarios, active fault lines exert significant control on PGA values. High-hazard zones are predominantly concentrated within the Longmenshan fault zone, with the southern area of Kangding also identified as a potential high-hazard region for landslides. Additionally, our research underscores that as the probability of exceedance decreases, the likelihood of earthquake-induced landslides and the extent of high-hazard areas increase significantly. Notably, the Pengguan complex rock mass in the southwest of the Longmenshan fault zone emerges as a particularly high-hazard area for coseismic landslides. The results provide critical data support for the spatial characterization and hazard zoning of earthquake-induced landslides in southwestern China. The insights gained from our research contribute valuable information for disaster preparedness and mitigation efforts in the region, helping to safeguard lives and infrastructure against seismic hazards.

Acknowledgements
Not applicable.

Author contributions
The research concept was proposed by CX, who also played a crucial role in data curation and analysis. XS designed the research framework, processed the relevant data, wrote the code and drafted the manuscript. SM, CX, JC, and WX actively participated in data analysis and SM made significant contributions to the revisions of the manuscript. All authors have carefully reviewed and approved the final version of the manuscript for publication in the manuscript.

Funding
This study was supported by the National Key Research and Development Program of China (2021YFB3901205), Aba Prefecture (including basin region) 1:250000 active fault project for (SAFE) the Sichuan Active Fault Exploration (No.: X-19-06) and the National Institute of Natural Hazards, Ministry of Emergency Management of China (ZDJ2020-14) and Young Elite Scientists Sponsorship Program by BAST (No. BYESS2023122).

Availability of data and materials
Data generated for seismically induced landslide hazard mapping of Aba Prefecture and Chengdu Plain region are mainly provided in the form of figures in the content of manuscript documents. Further, the influencing factors data and relevant codes for LR modeling are available upon request from the corresponding author. Also, the coseismic landslide inventories of Sichuan Province are available upon request from the corresponding author.

Declarations

Competing interests
The authors declare that they have no known competing financial interests or personal relationships that could have appeared to influence the work reported in this paper.

Author details
[1]National Institute of Natural Hazards, Ministry of Emergency Management of China, Beijing 100085, China. [2]Key Laboratory of Compound and Chained Natural Hazards Dynamics, Ministry of Emergency Management of China, Beijing 100085, China. [3]Key Laboratory of Landslide Risk Early-warning and Control, Ministry of Emergency Management of China, Chengdu 610059, China. [4]Key Laboratory of Active Tectonics and Volcano, Institute of Geology, China Earthquake Administration, Beijing 100029, China. [5]School of Earth Sciences and Resources, China University of Geosciences (Beijing), Beijing 100083, China.

Received: 10 June 2023 Accepted: 2 November 2023
Published online: 23 November 2023

References
Ahulu S, Danuor SK, Asiedu DK (2018) Probabilistic seismic hazard assessment of southern part of Ghana. J Seismolog 22:539–557
Allstadt KE, Jibson RW, Thompson EM, Massey CI, Wald DJ, Godt JW, Rengers FK (2018) Improving near-real-time coseismic landslide models: lessons learned from the 2016 Kaikōura, New Zealand, Earthquake. Bull Seismol Soc Am 108(3B):1649–1664

Anbalagan R (1992) Landslide hazard evaluation and zonation mapping in mountainous terrain. Eng Geol 32(4):269–277
Broeckx J, Vanmaercke M, Duchateau R, Poesen J (2018) A data-based landslide susceptibility map of Africa. Earth Sci Rev 185:102–121
Cao J, Zhang Z, Wang C, Liu J, Zhang L (2019) Susceptibility assessment of landslides triggered by earthquakes in the Western Sichuan Plateau. CATENA 175:63–76
Carrara A, Cardinali M, Guzzetti F, Reichenbach P (1995) GIS technology in mapping landslide hazard. In: Carrara A, Guzzetti F (eds) Geographical information systems in assessing natural hazards. Springer, Dordrecht, pp 135–175
Cellek S (2021) The effect of aspect on landslide and its relationship with other parameters Landslides. IntechOpen, Londan
Chen XL, Liu CG, Yu L, Lin CX (2014) Critical acceleration as a criterion in seismic landslide susceptibility assessment. Geomorphology 217:15–22
Chen Z, Huang Y, He X, Shao X, Li L, Xu C, Wang S, Xu X, Xiao Z (2023) Landslides triggered by the 10 June 2022 Maerkang earthquake swarm, Sichuan, China: spatial distribution and tectonic significance. Landslides 20:1–15
Cheng J, Xu X, Chen G (2020) A new prediction model of seismic hazard for the Sichuan-Yunnan region based on the occurrence rate of large earthquakes. J Geophys 63(3):1170–1182
Cornell CA (1968) Engineering seismic risk analysis. Bull Seismol Soc Am 58(5):1583–1601
Cui P, Chen X, Zhu Y, Su F, Wei F, Han Y, Liu H, Zhuang J (2009) The Wenchuan Earthquake (May 12, 2008), Sichuan Province, China, and resulting geohazards. Nat Hazards 56(1):19–36
Dai L, Scaringi G, Fan X, Yunus AP, Liu-Zeng J, Xu Q, Huang R (2021) Coseismic debris remains in the orogen despite a decade of enhanced landsliding. Geophys Res Lett 48(19):e2021GL095850
Deng Q (2007) Chinese active tectonic map. Seismological Press, Beijing
Fall M, Azzam R, Noubactep C (2006) A multi-method approach to study the stability of natural slopes and landslide susceptibility mapping. Eng Geol 82(4):241–263
Fan X, Scaringi G, Xu Q, Zhan W, Dai L, Li Y, Pei X, Yang Q, Huang R (2018) Coseismic landslides triggered by the 8th August 2017 Ms 7.0 Jiuzhaigou earthquake (Sichuan, China): factors controlling their spatial distribution and implications for the seismogenic blind fault identification. Landslides 15(5):967–983
Fan X, Scaringi G, Korup O, West AJ, van Westen CJ, Tanyas H, Hovius N, Hales TC, Jibson RW, Allstadt KE, Zhang L, Evans SG, Xu C, Li G, Pei X, Xu Q, Huang R (2019) Earthquake-induced chains of geologic hazards: patterns, mechanisms, and impacts. Rev Geophys 57(2):421–503
Fick SE, Hijmans RJ (2017) WorldClim 2: new 1-km spatial resolution climate surfaces for global land areas. Int J Climatol 37(12):4302–4315
Gao M (2021) Development and prospect of seismic zoning technology in China. City and Disaster Reduction 139(04):7–12
Hu Y (2002) Earthquake engineering in China. Earthq Eng Eng Vib 1(1):1–9
Hu Y, Wang Z, Liu G, Liu C, Fu Y (2017) Crustal structure imaging of multi-geophysical parameters and generating mechanisms of large earthquakes in North-South Seismic Zone. Chin J Geophys 60(6):2113–2129
Huang R, Fan X (2013) The landslide story. Nat Geosci 6(5):325–326
Huang Y, Xu C (2020) Analysis of the distribution law of landslides triggered by the Xingwen Ms5.7 earthquake in 2018. J Eng Geol 27:185–192
Huang Y, Xu C, Zhang X (2021a) Spatial distribution and influence factors of landslides triggered by the 2019 Ms 6.0 Changning, Sichuan, China Ms60 earthquake: a statistical analysis based on QGIS. IOP Conf Series Earth Environ Sci 861(5):052007
Huang Y, Xu C, Zhang X, Xue C, Wang S (2021b) An updated database and spatial distribution of landslides triggered by the Milin, Tibet Mw6.4 Earthquake of 18 November 2017. J Earth Sci 32(5):1069–1078
Huang Y, Xu C, Zhang X, Li L (2022) Bibliometric analysis of landslide research based on the WOS database. Natural Hazards Res 2(2):49–61
Jibson RW, Tanyaş H (2020) The influence of frequency and duration of seismic ground motion on the size of triggered landslides—a regional view. Eng Geol 273:105671
Jibson RW, Harp EL, Michael JA (2000) A method for producing digital probabilistic seismic landslide hazard maps: an example from the Los Angeles, California, area. Eng Geol 58(3–4):271–289
Kagan YY (2002) Seismic moment distribution revisited: II. Moment Conserv Principle Geophys J Int 149(3):731–754
Kavzoglu T, Sahin EK, Colkesen I (2014) Landslide susceptibility mapping using GIS-based multi-criteria decision analysis, support vector machines, and logistic regression. Landslides 11(3):425–439
Keefer DK (1984) Landslides caused by earthquakes. Geol Soc Am Bull 95(4):406–421
Kritikos T, Robinson TR, Davies TRH (2015) Regional coseismic landslide hazard assessment without historical landslide inventories: a new approach. J Geophys Res Earth Surf 120(4):711–729
Ling S, Sun C, Li X, Ren Y, Xu J, Huang T (2020) Characterizing the distribution pattern and geologic and geomorphic controls on earthquake-triggered landslide occurrence during the 2017 Ms 7.0 Jiuzhaigou earthquake, Sichuan China. Landslides 18(4):1275–1291
Liu JM, Wang T, Shi JS, Li ZT (2017) Emergency rapid assessment of landslides induced by the Jiuzhaigou Ms 7.0 earthquake, Sichuan China. J Geom 23(5):639–645
Lombardo L, Bakka H, Tanyas H, Westen C, Mai PM, Huser R (2019) Geostatistical modeling to capture seismic-shaking patterns from earthquake-induced landslides. J Geophys Res Earth Surf 124(7):1958–1980
Ma SY, Xu C (2019) Assessment of co-seismic landslide hazard using the Newmark model and statistical analyses: a case study of the 2013 Lushan, China, Mw66 earthquake. Nat Hazards 96(1):389–412
Ma S, Xu C, Shao X (2020) Spatial prediction strategy for landslides triggered by large earthquakes oriented to emergency response, mid-term resettlement and later reconstruction. Int J Disaster Risk Reduct 43:101362
Massey C, Townsend D, Rathje E, Allstadt KE, Lukovic B, Kaneko Y, Bradley B, Wartman J, Jibson RW, Petley DN, Horspool N, Hamling I, Carey J, Cox S, Davidson J, Dellow S, Godt JW, Holden C, Jones K, Kaiser A, Little M, Lyndsell B, McColl S, Morgenstern R, Rengers FK, Rhoades D, Rosser B, Strong D, Singeisen C, Villeneuve M (2018) Landslides triggered by the 14 November 2016 Mw 78 Kaikōura Earthquake, New Zealand. Bull Seismol Soc Am 108(3B):1630–1648
Merghadi A, Yunus AP, Dou J, Whiteley J, ThaiPham B, Bui DT, Avtar R, Abderrahmane B (2020) Machine learning methods for landslide susceptibility studies: a comparative overview of algorithm performance. Earth Sci Rev 207:103225
Meunier P, Hovius N, Haines AJ (2007) Regional patterns of earthquake-triggered landslides and their relation to ground motion. Geophys Res Lett. https://doi.org/10.1029/2007GL031337
Msilimba GG, Holmes PJ (2005) A landslide hazard assessment and vulnerability appraisal procedure: Vunguvungu/Banga Catchment. Northern Malawi Natural Hazards 34(2):199–216
Newmark NM (1965) Effects of earthquakes on dams and embankments. Géotechnique 15(2):139–160
Nowicki MA, Wald DJ, Hamburger MW, Hearne M, Thompson EM (2014) Development of a globally applicable model for near real-time prediction of seismically induced landslides. Eng Geol 173:54–65
Nowicki Jessee MA, Hamburger MW, Allstadt K, Wald DJ, Robeson SM, Tanyas H, Hearne M, Thompson EM (2019) A global empirical model for near-real-time assessment of seismically induced landslides. J Geophys Res Earth Surf 123(8):1835–1859
Papathanassiou G, Valkaniotis S, Ganas A (2021) Spatial patterns, controlling factors, and characteristics of landslides triggered by strike-slip faulting earthquakes: case study of Lefkada island, Greece. Bull Eng Geol Env 80(5):3747–3765
Parker RN, Densmore AL, Rosser NJ, de Michele M, Li Y, Huang R, Whadcoat S, Petley DN (2011) Mass wasting triggered by the 2008 Wenchuan earthquake is greater than orogenic growth. Nat Geosci 4(7):449–452
Parker RN, Rosser NJ, Hales TC (2017) Spatial prediction of earthquake-induced landslide probability. Nat Hazards Earth Syst Sci Discuss 2017:1–29
Pourghasemi HR, Gayen A, Park S, Lee C-W, Lee S (2018) Assessment of landslide-prone areas and their zonation using logistic regression, logitboost, and naïve Bayes machine-learning algorithms. Sustainability 10(10):3697
Reichenbach P, Rossi M, Malamud BD, Mihir M, Guzzetti F (2018) A review of statistically-based landslide susceptibility models. Earth Sci Rev 180:60–91
Robinson TR, Rosser NJ, Densmore AL, Williams JG, Kincey ME, Benjamin J, Bell HJA (2017) Rapid post-earthquake modelling of coseismic landslide intensity and distribution for emergency response decision support. Nat Hazards Earth Syst Sci 17(9):1521–1540
Rosser NJ, Robinson TR, Wilson TM, Davies TRH, Orchiston C (2018) Near-Real-Time modeling of landslide impacts to inform rapid response: an

example from the 2016 Kaikōura, New Zealand, Earthquake. Bull Seismol Soc Am 108(3B):1665–1682
Sajadi P, Sang Y-F, Gholamnia M, Bonafoni S, Mukherjee S (2022) Evaluation of the landslide susceptibility and its spatial difference in the whole Qinghai-Tibetan Plateau region by five learning algorithms. Geoscience Letters 9(1):9
Saleem N, Huq ME, Twumasi NYD, Javed A, Sajjad A (2019) Parameters derived from and/or used with digital elevation models (DEMs) for landslide susceptibility mapping and landslide risk assessment: a review. ISPRS Int J Geo Inf 8(12):545
Sana H (2019) A probabilistic approach to the seismic hazard in Kashmir basin NW Himalaya. Geosci Lett 6(1):5
Shao X, Xu C (2022) Earthquake-induced landslides susceptibility assessment: a review of the state-of-the-art. Natural Hazards Res 2(3):172–182
Shao X, Ma S, Xu C, Zhou Q (2020) Effects of sampling intensity and non-slide/slide sample ratio on the occurrence probability of coseismic landslides. Geomorphology 363:107222
Shao X, Xu C, Ma S, Shyu J, Zhou Q (2021) Calculation of landslide occurrence probability in Taiwan region under different ground motion conditions. J Mt Sci 18:1003–1012
Shao X, Xu C, Ma S (2022) Preliminary analysis of coseismic landslides induced by the 1 June 2022 Ms 61 Lushan Earthquake China. Sustainability 14(24):16554
Shao X, Ma S, Xu C (2023a) Distribution and characteristics of shallow landslides triggered by the 2018 Mw 75 Palu earthquake Indonesia. Landslides 20(1):157–175
Shao X, Ma S, Xu C (2023b) Hazard assessment modeling and software development of earthquake-triggered landslides in the Sichuan-Yunnan area China. Geosci Model Develop 16(17):5113–5129
Silva V, Crowley H, Pagani M, Monelli D, Pinho R (2014) Development of the openquake engine, the global earthquake model's open-source software for seismic risk assessment. Nat Hazards 72(3):1409–1427
Silva V, Amo-Oduro D, Calderon A, Costa C, Dabbeek J, Despotaki V, Martins L, Pagani M, Rao A, Simionato M, Viganò D, Yepes-Estrada C, Acevedo A, Crowley H, Horspool N, Jaiswal K, Journeay M, Pittore M (2020) Development of a global seismic risk model. Earthq Spectra 36:372–394
Tanyas H, Rossi M, Alvioli M, van Westen CJ, Marchesini I (2019) A global slope unit-based method for the near real-time prediction of earthquake-induced landslides. Geomorphology 327:126–146
Tateishi R, Uriyangqai B, Al-Bilbisi H, Ghar MA, Tsend-Ayush J, Kobayashi T, Kasimu A, Hoan NT, Shalaby A, Alsaaideh B, Enkhzaya T, Gegentana SHP (2011) Production of global land cover data—GLCNMO. Int J Digital Earth 4(1):22–49
Tian Y, Xu C, Xu X, Chen J (2016) Detailed inventory mapping and spatial analyses to landslides induced by the 2013 Ms 66 Minxian earthquake of China. J Earth Sci 27(6):1016–1026
Tian Y, Xu C, Ma S, Xu X, Wang S, Zhang H (2019) Inventory and spatial distribution of landslides triggered by the 8th August 2017 MW 65 Jiuzhaigou Earthquake China. J Earth Sci 30(1):206–217
Van Westen CJ, Seijmonsbergen AC, Mantovani F (1999) Comparing landslide hazard maps. Nat Hazards 20(2):137–158
Vorpahl P, Elsenbeer H, Märker M, Schröder B (2012) How can statistical models help to determine driving factors of landslides? Ecol Model 239:27–39
Wang Z, Zhao D, Wang J (2010) Deep structure and seismogenesis of the north-south seismic zone in southwest China. J Geophys Res Solid Earth. https://doi.org/10.1029/2010JB007797
Wang T, Liu J, Li Z, Xin P, Shi J, Wu S (2021) Seismic landslide hazard assessment of China and its impact on national territory spatial planning. Geology in China 48(1):21–39
Watkinson IM, Hall R (2019) Impact of communal irrigation on the 2018 Palu earthquake-triggered landslides. Nat Geosci 12(11):940–945
Wen X (2001) Earthquake behavior of variable rupture-scale on active faults and application of the cascade-rupturing model. Acta Seismol Sin 23(4):380–390
Wu W, Xu C, Wang X, Tian Y, Deng F (2020) Landslides triggered by the 3 August 2014 Ludian (China) Mw 62 earthquake: an updated inventory and analysis of their spatial distribution. J Earth Sci 31(4):853–866
Xiong J, Chen M, Tang C (2021) Long-term changes in the landslide sediment supply capacity for debris flow occurrence in Wenchuan County. China Catena 203:105340
Xu C, Xu X (2014) Statistical analysis of landslides caused by the Mw 69 Yushu, China, earthquake of 2010. Nat Hazards 72(2):871–893
Xu C, Xu X, Yao X, Dai F (2014) Three (nearly) complete inventories of landslides triggered by the May 12, 2008 Wenchuan Mw 79 earthquake of China and their spatial distribution statistical analysis. Landslides 11(3):441–461
Xu C, Xu X, Shyu JBH (2015) Database and spatial distribution of landslides triggered by the Lushan, China Mw 6.6 earthquake of 20 April 2013. Geomorphology 248:77–92
Xu X, Han Z, Yang X (2016) Seismotectonic map in China and its adjacent regions. Seismological Press, Beijing
Xu C, Xu X, Zhou B, Shen L (2019) Probability of coseismic landslides: a new generation of earthquake-triggered landslide hazard model. J Eng Geol 27(5):1122
Yang Z, Xu C, Li L (2022a) Landslide detection based on ResU-Net with transformer and CBAM embedded: two examples with geologically different environments. Remote Sensing 14(12):2885
Yang Z, Xu C, Shao X, Ma S, Li L (2022b) Landslide susceptibility mapping based on CNN-3D algorithm with attention module embedded. Bull Eng Geol Env 81(10):412
Yin Y, Wang F, Sun P (2009) Landslide hazards triggered by the 2008 Wenchuan earthquake, Sichuan China. Landslides 6(2):139–152
Zhao B, Huang Y, Zhang C, Wang W, Tan K, Du R (2015) Crustal deformation on the Chinese mainland during 1998–2014 based on GPS data. Geodesy Geodynam 6(1):7–15
Zhao B, Wang Y, Li W, Su L, Lu J, Zeng L, Li X (2021) Insights into the geohazards triggered by the 2017 Ms 69 Nyingchi earthquake in the east Himalayan syntaxis China. CATENA 205:105467
Zhao B, Hu K, Yang Z, Liu Q, Zou Q, Chen H, Zhang W, Zhu L, Su L-J (2022) Geomorphic and tectonic controls of landslides induced by the 2022 Luding earthquake. J Mt Sci 19(12):3323–3345

Publisher's Note